Semicond. Sci. Technol. **13** (1998) 714–724. Printed in the UK PII: S0268-1242(98)91145-2

Microscopic analysis of shot-noise suppression in nondegenerate ballistic transport

T González†, J Mateos†, D Pardo†, O M Bulashenko‡ and L Reggiani§

† Departamento de Física Aplicada, Universidad de Salamanca, Plaza de la Merced s/n, E-37008 Salamanca, Spain
‡ Departament de Física Fonamental, Universitat de Barcelona, Av. Diagonal 647, E-08028 Barcelona, Spain
§ Istituto Nazionale di Fisica della Materia, Dipartimento di Scienza dei Materiali, Università di Lecce, Via Arnesano, 73100 Lecce, Italy

Received 29 January 1998, accepted for publication 7 April 1998

Abstract. We present a numerical simulation of shot-noise suppression due to long-range Coulomb interaction in nondegenerate ballistic transport. Calculations make use of an ensemble Monte Carlo simulator self-consistently coupled with a one-dimensional Poisson solver, and are applied to a ballistic semiconductor structure formed of a lightly doped active region surrounded by two contacts acting as reservoirs. The doping of the injecting contacts and the applied voltage are taken as variable parameters. At increasing voltages the transition from thermal to shot-noise conditions is analysed. Space-charge is found to be responsible for an important suppression of shot noise even in the presence of linear current–voltage characteristics. At increasing injection rates we have found a strong tendency towards shot-noise suppression which scales with a dimensionless Debye length. The statistical properties of the electron flow along the structure are modified by Coulomb interaction, evidencing a sub-Poissonian behaviour. The frequency dependence of the fluctuations is also analysed. The spectral density of current fluctuations exhibits structures related to the different characteristic times involved in the carrier transport.

1. Introduction

Shot noise is caused by the randomness in the flux of carriers crossing the active region of a given device and is associated with the discreteness of the electric charge [1]. At low frequency (small compared to the inverse of the transit time through the active region) the power spectral density of shot noise is given by $S_I = \gamma 2qI$, where I is the d.c. current, q the electron charge and γ the suppression factor. When carriers cross the active region in an uncorrelated way, full shot noise with $\gamma = 1$ is observed, which indicates that the current pulses follow a Poissonian distribution. However, correlations between carriers can reduce the shot-noise value giving $\gamma < 1$, and leading to binomial [2, 3], sub-Poissonian [4] or other kinds of statistics [5]. In recent years the study of shot-noise suppression in low-dimensional and mesoscopic systems [6] has attracted increasing attention from both a theoretical [7–20] and an experimental [21–31] point of view. Since it can be used to obtain additional information which is not available from d.c. characteristics or low-frequency conductance, shot-noise investigation has become a fundamental tool for the understanding of electron transport in low-dimensional and mesoscopic devices.

Several mechanisms can be responsible for introducing correlations between electrons in different systems. Among them we recall: the Pauli exclusion principle under degenerate conditions in systems obeying Fermi statistics [21, 24–27]; short-range Coulomb interaction (electron–electron scattering), where a $\sqrt{3}/4$ suppression factor has been predicted [16, 17]; tunnelling transport, where a $\frac{1}{2}$ noise-suppression factor has been found in symmetric double-barrier junctions [21, 24, 25, 32]; coherent and diffusive conductors, where a $\frac{1}{3}$ suppression has been demonstrated [10, 11, 13, 20, 28, 33]. Another possible way of incorporating the correlation among carriers is by means of long-range Coulomb repulsion (through the self-consistent electric potential) [4, 33–35]. While most of the above mechanisms have been extensively discussed in solid-state literature [6], the last one has received less attention [36–38], although its relevance to shot-noise suppression has been known since the era of vacuum tube devices [39].

The suppression due to Coulomb interaction can be achieved by virtue of a potential barrier near an injecting

0268-1242/98/070714+11$19.50

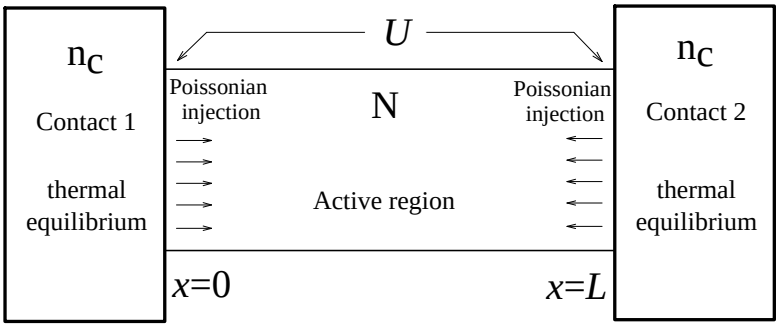

Figure 1. Schematic drawing of the ballistic structure under investigation.

contact which fluctuates synchronously with electron passage through it. In this way, an incoming Poissonian flow is converted into an outgoing sub-Poissonian flow [4]. This effect is similar to that leading to shot-noise suppression in vacuum diodes and discussed in the literature long ago [40], although, in the case of solid-state devices, the potential barrier should not necessarily be provided by space-charge. In a semiconductor structure it might be, for example, caused by a constriction, as in the experiment on a quantum point contact by Reznikov *et al* [26]. We notice that although the importance of Coulomb correlations on noise suppression in mesoscopic structures has been emphasized [8, 12, 14, 18], under ballistic transport regime only a few calculations where the dynamic potential fluctuations are taken into account are available [4, 34, 36].

The aim of the present paper is to investigate the effect of long-range Coulomb interaction on the shot-noise power spectrum *under nondegenerate ballistic regime of carrier transport* in a two-terminal device, thus completing and extending preliminary reports on the subject [4, 34]. The ballistic regime is nowadays accessible in mesoscopic devices such as electron waveguides, quantum point contacts etc, with characteristic lengths of the order of, or smaller than, the carrier mean free path. The theories which are used to interpret the experiments on shot-noise suppression [22, 26, 27] commonly neglect the contribution coming from the fluctuations of the self-consistent potential. Here, we use a rigorous microscopic approach by self-consistently coupling an ensemble Monte Carlo simulator with a Poisson solver (PS) [41] thus giving a theoretical frame for the understanding of specific experimental results. We address the case, typical of semiconductors, of a sufficiently low carrier concentration thus avoiding any effect due to statistical degeneracy. This approach allows us also to calculate the frequency dependence of shot noise, a subject which is usually disregarded, though recently receiving renewed attention [37, 38].

The outline of the paper is as follows. In section 2 we discuss the physical model used for the ballistic structures, with special emphasis on the modelling of the contacts. We also provide the details of the Monte Carlo simulation and noise calculations. Section 3 presents the results of the present investigation and will be concerned with static characteristics, the shot-noise suppression and the frequency dependence of the noise spectrum. Finally, in section 4 the main conclusions and future trends of the present work are summarized.

2. Physical model

In this section we present the details of the structures here analysed, the models used in the simulations and the procedures for the noise calculation.

2.1. Simulated structure

For our analysis we consider the simple semiconductor structure shown in figure 1. It consists of a lightly doped active region of a semiconductor sample sandwiched between two heavily doped contacts (of the same semiconductor) which act as reservoirs by injecting carriers into the active region. The doping of the contacts is always taken to be much higher than that of the sample. The carrier density at the contacts, n_c, corresponds to their doping concentration; all impurities are assumed to be ionized at the temperature considered. The contacts are considered to be ohmic (the voltage drop inside them is negligible) and they remain always at thermal equilibrium. Accordingly, when a voltage U is applied to the structure, all the potential drop takes place inside the active region, between the positions $x = 0$ and $x = L$. The electron mean free path ℓ is assumed to be much longer than the distance L between the contacts, and therefore carrier transport is ballistic inside the active region. The structure then acts similarly to a vacuum diode, with the relevant difference that there are two opposing currents, instead of a single one, which flow in the presence of a medium. We shall analyse six different structures where, while the length of the sample remains unchanged, the doping of the contacts is modified.

2.2. Monte Carlo simulation

The transport analysis is carried out by simulating the carrier dynamics only in the active region of the structure. The influence of the contacts is included in the simulation by means of a stochastic injection rate taking place at positions $x = 0$ and $x = L$. Under the action of a d.c. applied voltage U, the carrier dynamics are simulated by an ensemble Monte Carlo technique self-consistently coupled

with a PS [41]. The simulation is one-dimensional in real space (the Poisson equation is solved only in the direction of the applied voltage) and fully three-dimensional in momentum space. Since we are interested in analysing only the effects related to the Coulomb interaction, the electron gas inside the sample is assumed to be nondegenerate, thus excluding any additional correlations due to Fermi statistics. The carriers move ballistically inside the active region according to the semiclassical equations of motion with a constant effective mass. Under the condition of a constant applied voltage, the instantaneous current in a one-dimensional structure is given by [42]

$$I(t) = \frac{q}{L}\sum_{i=1}^{N(t)} v_i(t) \tag{1}$$

where $N(t)$ is the number of particles inside the structure and $v_i(t)$ the velocity component along the field direction of the ith particle. It must be stressed that, although not explicitly appearing in (1), the displacement current is implicitly taken into account by constant-voltage conditions [42].

To better analyse the importance of Coulomb correlations we provide the results for two different simulation schemes. The first one involves a *dynamic* PS, which means that any fluctuation of space-charge due to the random injection from the contacts causes a redistribution of the potential, which is self-consistently updated by solving the Poisson equation at each time step during the simulation to account for the fluctuations associated with the long-range Coulomb interaction. The second scheme uses a *static* PS to calculate only the stationary potential profile; i.e. once the steady state is reached, the PS is switched off, so that carriers move in the *frozen* non-fluctuating electric field profile. Both schemes are checked to give exactly the same steady-state spatial distributions and total current, but the noise characteristics and the statistical distributions of transmitted carriers are different. Of course, the PS scheme which is physically correct is the dynamic one. The static case is just used to evaluate quantitatively the influence of the self-consistent potential fluctuations on the total noise.

For the calculations we have used the following set of parameters: lattice temperature $T = 300$ K, electron effective mass, $m = 0.25m_0$, dielectric constant $\epsilon = 11.7\epsilon_0$, sample length $L = 2000$ Å, contact doping n_c ranging between 10^{13} cm^{-3} and 4×10^{17} cm^{-3} and doping of the active region $n_{ar} = 10^{11}$ cm^{-3}. As proved in the appendix, with the above model the results on shot-noise suppression depend only on the dimensionless length λ, defined as

$$\lambda = \frac{L}{L_{Dc}} \tag{2}$$

where

$$L_{Dc} = \sqrt{\frac{\epsilon k_B T}{q^2 n_c}} \tag{3}$$

is the Debye length corresponding to the carrier concentration at the contact, with k_B the Boltzmann constant.

Typical values of the time step and number of meshes in real space used for the PS are 2 fs and 100 respectively. We have checked that by reducing the time step or by increasing the number of meshes the results remain the same. The average number of simulated particles in the active region ranges between 50 and 2000 depending on the contact doping and applied voltage.

2.3. Contact model

Since the carrier motion in the active region of the structures is ballistic, the behaviour of the contacts is crucial in determining the current noise. To provide a complete model for the contacts and define the sources of randomness in the carrier flux associated with them, we have to specify the velocity distribution of the injected carriers $f_{inj}(\boldsymbol{v})$, the injection rate Γ and its statistical properties. Here we have denoted $\boldsymbol{v} \equiv (v_x, v_y, v_z)$.

Let us consider the process of electron injection from contact 1 into the active region at $x = 0$ (see figure 1). According to equilibrium conditions at the contacts, the injected carriers follow a Maxwellian distribution weighted by the velocity component v_x normal to the surface of the contact

$$f_{inj}(\boldsymbol{v}) = v_x f_{MB}(\boldsymbol{v}) \qquad v_x > 0 \tag{4}$$

where $f_{MB}(\boldsymbol{v})$ is the Maxwell–Boltzmann distribution at the lattice temperature. The injection rate Γ, i.e. the number of carriers per unit time which are entering the sample, is given by

$$\Gamma = n_c \bar{v}_+ S \tag{5}$$

where S is the cross-sectional area of the device, and

$$\bar{v}_+ = \int_0^\infty \int_{-\infty}^\infty \int_{-\infty}^\infty f_{inj}(\boldsymbol{v})\,\mathrm{d}v_x\,\mathrm{d}v_y\,\mathrm{d}v_z = \sqrt{\frac{k_B T}{2\pi m}}. \tag{6}$$

This injection rate is considered to be independent of the applied voltage. Due to the very high value of n_c as compared with the sample doping, any possible influence of the applied voltage (especially for high values) on the contact and, consequently, on the injection rate, is neglected. Therefore, the maximum current I_S (saturation current) that a contact can provide will then be given by

$$I_S = q\Gamma. \tag{7}$$

As the transport regime in the active region is ballistic (i.e. deterministic), shot noise originates from the random injection at the contacts, which is taken to follow Poissonian statistics. Accordingly, the time between two consecutive electron injections t_{inj} is generated with a probability per unit time given by

$$P(t_{inj}) = \Gamma \mathrm{e}^{-\Gamma t_{inj}}. \tag{8}$$

In the simulation we make use of (8) to determine t_{inj}, which, following the Monte Carlo technique, is given by

$$t_{inj} = -\frac{1}{\Gamma}\ln(r) \tag{9}$$

where r is a random number uniformly distributed between 0 and 1. We note that the carrier number in the sample $N(t)$ is a stochastic quantity and electrons are injected at

$x = 0$ and $x = L$ into the active region of the structure according to the above fluctuating rate. When a carrier exits through any of the contacts it is cancelled from the simulation statistics, which account only for the carriers that are inside the active region at the given time t. Thus $N(t)$ fluctuates in time due to the random injection from the contacts and we evaluate both the time-averaged value $\langle N\rangle$ and its fluctuations $\delta N(t) = N(t) - \langle N\rangle$.

In the contact model previously described we are assuming that the doping of the contacts is so high compared with that of the active region that all the built-in effects associated with the diffusion of carriers around the contacts take place exclusively in the active region. As a consequence, the model is not fully consistent, since the effects related to the possible fluctuations of the concentration at the contacts are not included in the calculation of the current according to (1). In any case we are mostly interested in the low-frequency region of the noise spectrum, and these effects (like plasma oscillations [43]) are expected to appear at very high frequencies, beyond the cut-off region of shot noise.

Several values of n_c (and therefore several injection rates Γ) are considered. As n_c increases, space-charge effects become more and more relevant, the dimensionless parameter λ being the indicator of their importance. In particular, we have considered the following values of n_c (in cm^{-3}, with the corresponding λ): 10^{13}, $\lambda = 0.15$; 2×10^{15}, $\lambda = 2.18$; 10^{16}, $\lambda = 4.88$; 2.5×10^{16}, $\lambda = 7.72$; 10^{17}, $\lambda = 15.45$; 4×10^{17}, $\lambda = 30.90$. These values of n_c cover the range from negligible ($\lambda = 0.15$) to very important effects played by long-range Coulomb interaction ($\lambda = 30.9$) †. It should be noted that the boundary condition at the contact can be defined either through the contact electron density n_c or, equivalently, through the injection rate Γ, as they are proportional. We use the former since it allows us to introduce the characteristic screening parameter L_{Dc} associated with n_c (equation (3)), which completely determines the importance of space-charge effects inside the active region. In such a case, the shot-noise suppression can be characterized in terms of the dimensionless length $\lambda = L/L_{Dc}$.

2.4. Noise calculation

In our analysis of shot noise we are mostly interested in calculating the low-frequency value of the spectral density of current fluctuations $S_I(0)$. To this end, from the simulation we firstly evaluate the autocorrelation function of current fluctuations, $\delta I(t) = I(t) - \langle I\rangle$, which under stationary conditions is given by

$$C_I(t) = \langle \delta I(0)\, \delta I(t)\rangle \tag{10}$$

which, after Fourier transformation, provides the spectral density

$$S_I(f) = 2\int_{-\infty}^{\infty} C_I(t) \mathrm{e}^{\mathrm{i}2\pi f t}\, \mathrm{d}t. \tag{11}$$

† The same values of λ (and therefore the same shot-noise suppression results) could be obtained by keeping n_c constant and appropriately modifying L according to (2) and (3).

Once a sufficiently long sequence of current values $I(t)$ is obtained from the simulation, the time average of the current $\langle I\rangle$ is determined and the current autocorrelation function is easily calculated following (10). To clarify the role of different contributions to the current noise we decompose the current autocorrelation function and the spectral density into three main contributions as

$$C_I(t) = C_V(t) + C_N(t) + C_{VN}(t) \tag{12}$$

respectively given by

$$C_V(t) = \frac{q^2}{L^2}\langle N\rangle^2 \langle \delta v(t')\, \delta v(t'+t)\rangle \tag{13a}$$

$$C_N(t) = \frac{q^2}{L^2}\langle v\rangle^2 \langle \delta N(t')\, \delta N(t'+t)\rangle \tag{13b}$$

$$C_{VN}(t) = \frac{q^2}{L^2}\langle v\rangle\langle N\rangle \langle \delta v(t')\, \delta N(t'+t) + \delta N(t')\, \delta v(t'+t)\rangle. \tag{13c}$$

In the above equations C_V is associated with fluctuations in the mean carrier velocity, C_N with fluctuations in the carrier number and C_{VN} with their cross-correlation [41, 42]. To distinguish between the results obtained by using static and dynamic PSs, we shall denote the corresponding current spectral densities as S_I^s and S_I^d respectively.

3. Results

3.1. Static characteristics

Figure 2 shows the electron concentration and potential profiles inside the active region for several values of λ under thermodynamic equilibrium conditions. As λ increases, the higher injection rate at the contacts leads to a larger carrier concentration inside the sample and to a stronger nonuniformity of its spatial distribution, showing maximum values at the contacts due to the electron injection and decaying towards the middle of the sample. Accordingly, the potential profile exhibits a minimum in the middle of the active region of amplitude V_m which increases with λ, thus evidencing the stronger influence of space-charge. For the highest value of λ, V_m reaches $4k_BT/q$. When a positive voltage is applied to the anode (contact 2 in figure 1), the minimum is displaced towards the cathode (contact 1) while its amplitude decreases, as shown in figure 3 for the case of $\lambda = 30.9$. Physically, this minimum provides a potential barrier for the electron moving between the contacts. Accordingly, the injected electrons not having sufficient energy to pass the barrier are reflected back to the contacts. The mechanism of shot-noise suppression is based on the fact that the barrier height and, as a consequence, the transmission through it, fluctuate with the passage of electrons and modify the Poissonian statistics of the incoming carriers. Therefore, the transmission through the barrier is current dependent, which is crucial in calculating the noise characteristics. Of course, the fluctuations of the barrier are more important when stronger space-charge effects are present (high λ).

Figure 4 shows the dependence of the current I, average energy ε and average number of electrons inside the active

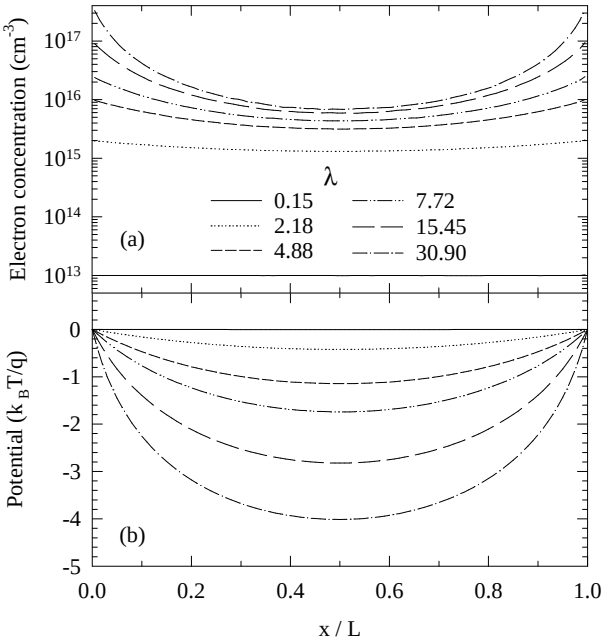

Figure 2. Spatial profiles along the active region of (a) electron concentration and (b) normalized potential $q\phi(x)/k_BT$ at equilibrium for different values of λ.

region N with the applied voltage U for different values of λ. The current flowing through the diode reflects the evolution of V_m with U shown in figure 3. The current I consists of two opposite contributions

$$I = I^+ - I^- \tag{14}$$

I^+ flowing from the cathode to the anode and I^- in the opposite direction. Since the injected carriers follow a Maxwellian distribution and move ballistically, the value of both currents depends exponentially on the amplitude of the potential barrier that the carriers injected at each contact find when moving towards the opposite contact. For I^+ the amplitude is just V_m and for I^- it is $V_m + U$. Therefore

$$I^+ = I_S \exp[-qV_m/k_BT] \tag{15a}$$
$$I^- = I_S \exp[-q(V_m + U)/k_BT]. \tag{15b}$$

As a result, while the presence of the minimum V_m persists, the current increases practically linearly with U, up to a certain value of the external bias U_{sat} for which the barrier vanishes, so that all the electrons injected at the cathode can reach the anode, the current saturates and becomes independent of the bias (figure 4(a)). As λ is increased, the barrier induced by the space-charge is more important, the current is lower and the saturation takes place for higher applied voltages. In the case of λ = 0.15, when space-charge effects are negligible, the I–U curve corresponds exactly to that obtained in [44] within an approach where Coulomb correlations are disregarded. The dependence of the carrier average energy on U (figure 4(b)) shows the cooling effect associated with the presence of V_m. Starting from $U \sim k_BT/q$, the increase of the average energy with U is systematically lower for higher values of λ. When V_m

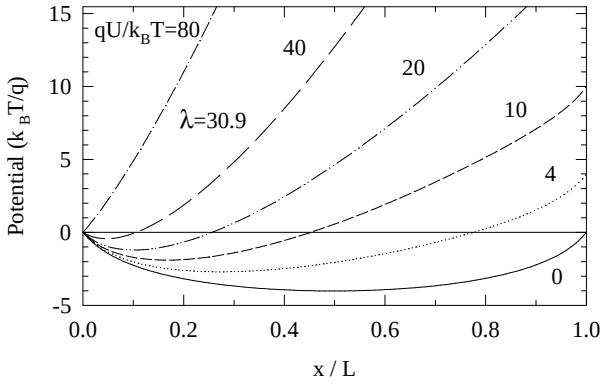

Figure 3. Spatial profiles of the normalized potential $q\phi(x)/k_BT$ for different applied voltages U (in units of k_BT/q) for the case of λ = 30.9. Note the evolution of the amplitude and position of the potential minimum until its disappearance at the highest applied voltages.

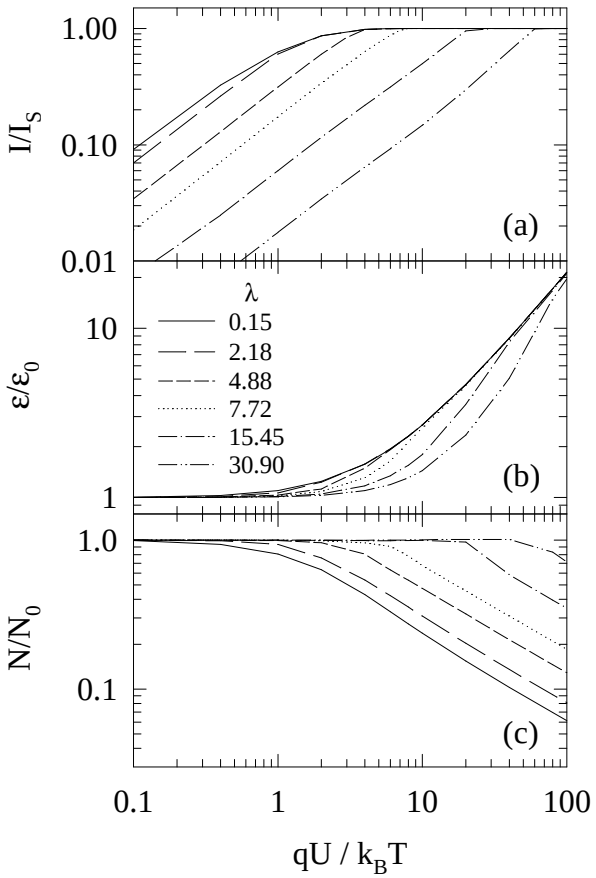

Figure 4. (a) Current flowing through the sample normalized to the saturation value, (b) average energy of electrons inside the active region normalized to the thermal value and (c) carrier number inside the active region normalized to the equilibrium value as a function of the applied voltage for several values of λ.

vanishes, current saturation conditions are reached, and the average energy becomes independent of λ by approaching a linear increase with the applied voltage [45]. In figure 4(c) it can be observed that the voltage dependence of N/N_0

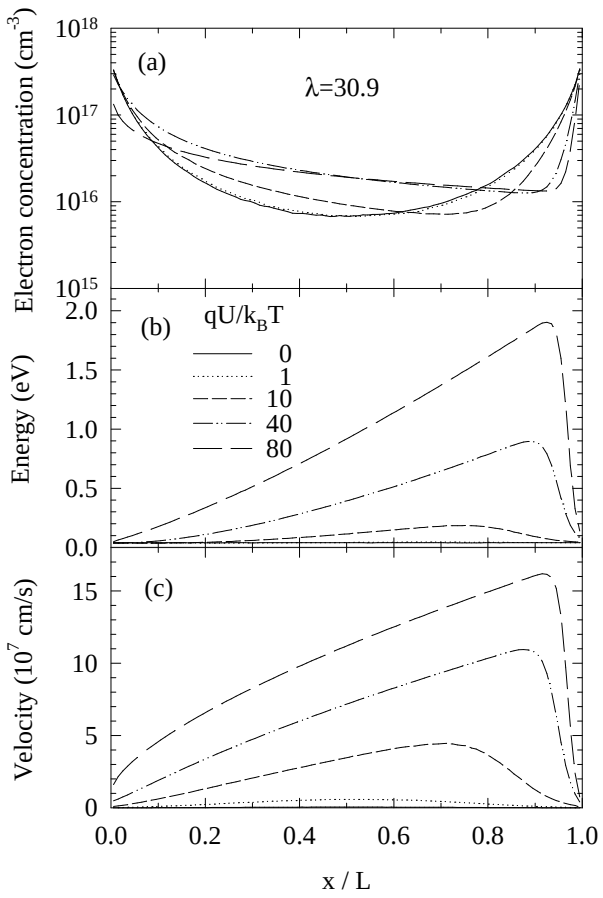

Figure 5. Spatial profiles along the sample of (a) electron concentration, (b) average energy and (c) average velocity for the case λ = 30.9 at several applied voltages.

mirrors that of I/I_s; N decreases systematically with the voltage ($\sim U^{-1/2}$) once the current is saturated.

Figure 5 shows the profiles of the electron concentration n, carrier average energy ε and velocity v along the active region of the structure with $\lambda = 30.9$ for several values of U. When a voltage is applied to the right contact, the symmetry of the carrier concentration profile at equilibrium is clearly destroyed in order to ensure current conservation through the sample. Accordingly, near the anode, where v reaches the highest values, n takes the lowest ones. The extension of the region near the anode contact where the carrier concentration is high and both the velocity and energy are low decreases at increasing applied voltages. In this region, most of the carriers are thermal electrons proceeding from the right contact which are reflected back to the anode by the opposite electric field. The greater the applied voltage, the higher the opposite field and the shorter the distance they penetrate before being reflected. When U is high and the potential barrier is near to disappearing or has just vanished (see figure 3, $U = 40$, $80k_BT/q$) the energy increases systematically along the sample up to a maximum value close to qU near the anode contact, as expected from the ballistic transport inside the sample.

The velocity distribution of the carriers inside the active region of the structure with $\lambda = 30.9$ is shown in figure 6 for several applied voltages. At equilibrium, the expected Maxwellian distribution at the lattice temperature is found. As U is increased, the fraction of carriers with negative velocities is reduced and the distribution is displaced to positive velocities. The Maxwellian shape of the distribution is conserved until high values of U are applied ($qU \gg k_BT$), for which a significant tail of high positive-velocity carriers induced by the field acceleration is present. When the potential barrier disappears ($U = 80k_BT/q$, see figure 3), all the carriers injected by the left contact have positive velocities inside the active region (none is reflected back) and the only carriers with negative velocities are those injected at the anode contact. This leads to the shape of the distribution around zero velocity showing two different slopes.

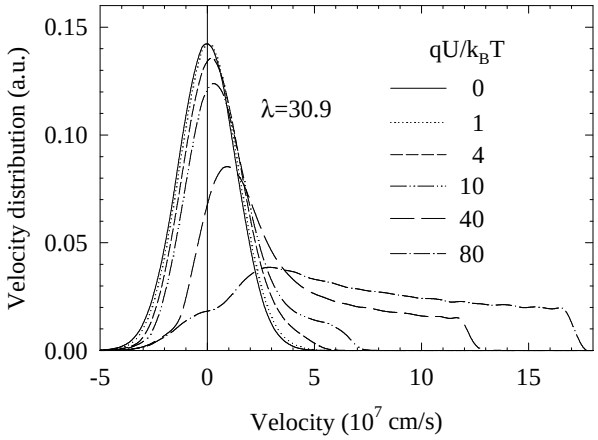

Figure 6. Distribution function of the carrier velocity inside the active region for λ = 30.9 at several applied voltages.

All the results presented in this section are independent of the PS scheme used for the calculations.

3.2. Shot-noise suppression

Once the static characteristics have been analysed, the shot-noise suppression effects can be more easily understood. Below, the difference between the results of the static and dynamic PS will evidence the influence of the dynamic fluctuations of the potential on the noise characteristics of the structures. As we have already mentioned, the number of carriers instantaneously present in the active region of the structures fluctuates in time. Its variance normalized to the number of carriers at equilibrium $\langle \Delta N^2 \rangle / N_0$ is shown in figure 7 as a function of the applied voltage for $\lambda = 7.72$. When the static PS is used, $\langle \Delta N^2 \rangle$ coincides exactly with the average carrier number N. This is the expected result, since in the absence of dynamic Coulomb correlations and other sources of noise inside the sample, the carrier number follows the Poissonian statistics imposed by the contacts. However, in the case of dynamic calculations, a sub-Poissonian behaviour is observed, $\langle \Delta N^2 \rangle$ being significantly smaller than N in the complete range of applied voltages for which the potential barrier is present. Only after current saturation (see figure 4(a)), that is when the potential barrier vanishes, does $\langle \Delta N^2 \rangle$ return to the Poissonian value.

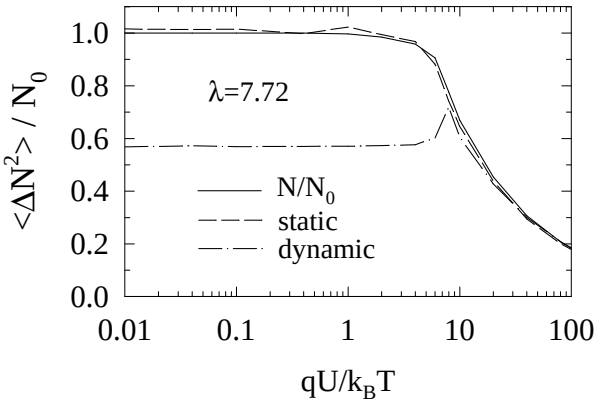

Figure 7. Variance of carrier number inside the active region normalized to the carrier number at equilibrium as a function of the applied voltage for the case λ = 7.72, calculated by using static and dynamic PSs. The normalized average carrier number is also plotted for comparison.

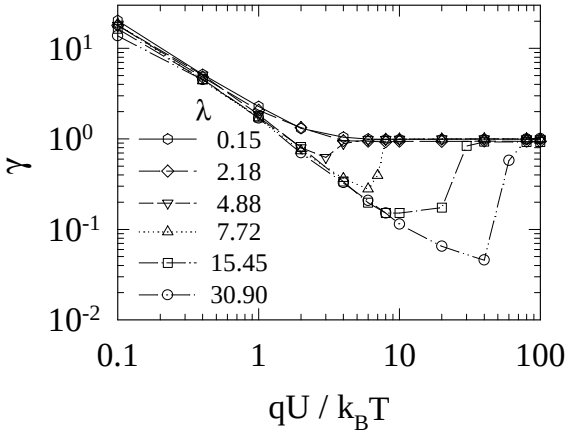

Figure 8. Shot-noise suppression factor $\gamma = S_I^d/2qI$ versus applied voltage for several values of λ.

After having proved that the carrier statistics are modified by Coulomb correlations, we analyse their influence on the low-frequency value of the current spectral density S_I. In the static case, S_I^s should be given by the sum of the full shot noise associated with the two opposite currents flowing through the structure. Accordingly, at all voltages and for all the values of λ analysed, we obtain an excellent coincidence [34] of S_I^s with the standard formula used to describe the crossover from thermal to shot noise when carrier correlations play no role [1]

$$S_I = 2q(I^+ + I^-) = 2qI\coth(qU/2k_BT) \qquad (16)$$

where I is the total current flowing through the structure given by (14) and (15). This agreement confirms the validity of the simulation scheme used for the calculations. For the lowest values of λ (0.15, 2.18) no difference between the dynamic and static cases is obviously detected. Indeed, for $\lambda = 0.15$, S_I^s and S_I^d coincide exactly, with values in complete agreement with those obtained in [44] in the absence of Coulomb correlations. However, at increasing values of λ, when space-charge effects become significant, starting from $qU \sim k_BT$, S_I^d decreases with respect to S_I^s (which in this range, according to (16), corresponds to full shot noise $S_I^s \approx 2qI$) and exhibits a minimum before jumping to the saturation value [34]. Under saturation, the results for both schemes coincide and full shot noise is recovered in the dynamic case $S_I^d = S_I^s = 2qI_s$ (no barrier modulating the current). When compared with the static case, the noise suppression is stronger for higher λ (more important space-charge effects).

This behaviour of S_I is illustrated in figure 8, where the suppression factor $\gamma = S_I^d/2qI$ is shown as a function of U for different λ. The sequence of thermal-noise (for $qU < k_BT$), suppressed shot-noise (for $k_BT < qU < qU_{sat}$) and full shot-noise ($U > U_{sat}$) behaviour is clearly shown. The curves corresponding to the different structures only differ in the suppressed-shot-noise range. For the lowest values of λ, when no suppression takes place, $\gamma = \coth(qU/2k_BT)$. Shot-noise reduction becomes more pronounced and covers a wider range as λ increases (e.g. for $\lambda = 30.9$, $\gamma = 0.045$). Thus, the present self-consistent approach predicts values of the suppression factor much lower than those of previous analytical models [36] where the dependence of the potential minimum and its position on the applied voltage was not taken into account. The reduced shot-noise level found with our approach is accompanied by sub-Poissonian electron number statistics, as was reported in [4]. We stress that, according to the results shown in figure 7, Coulomb correlations modify the statistical properties of the carrier-number fluctuations even under thermal equilibrium conditions. However, their influence on the current noise (as an excess noise contribution) is evidenced only in the presence of a net current when the noise goes from the thermal to the shot-noise limit ($qU > k_BT$).

In principle, the value of γ has no lower limit and it follows asymptotically the behaviour $\gamma \sim k_BT/qU$ in the range $k_BT < qU < qU_{sat}$. Furthermore, through λ, γ can reach values as low as desired by an appropriate increasing of the sample length and/or the carrier concentration at the contacts, provided the transport remains ballistic. However, by increasing the device length (or the lattice temperature) the carrier transport actually goes from a ballistic to a diffusive regime and the action of Coulomb interaction on shot-noise suppression changes completely [35]. Moreover, when the carrier concentration at the contact is increased so that the electron gas becomes degenerate, statistical (Pauli) correlations between carriers act as an additive contribution to shot-noise suppression.

To better understand the physical reason for shot-noise suppression in the present ballistic structure, figure 9 reports the decomposition of S_I into the three additive contributions S_V, S_N and S_{VN} (equations (13)) for $\lambda = 7.72$ and different U. Both S_N and S_{VN} vanish at equilibrium ($U \to 0$), since they are proportional to $\langle v\rangle^2$ and $\langle v\rangle \to 0$. Thus, for small biases ($qU \ll k_BT$) $S_I \sim S_V$, which means that the current noise is the thermal noise associated with velocity fluctuations and governed by the Nyquist theorem $S_I^s = S_I^d \approx 4k_BTG$, with $G = \mathrm{d}I/\mathrm{d}V|_{V=0}$

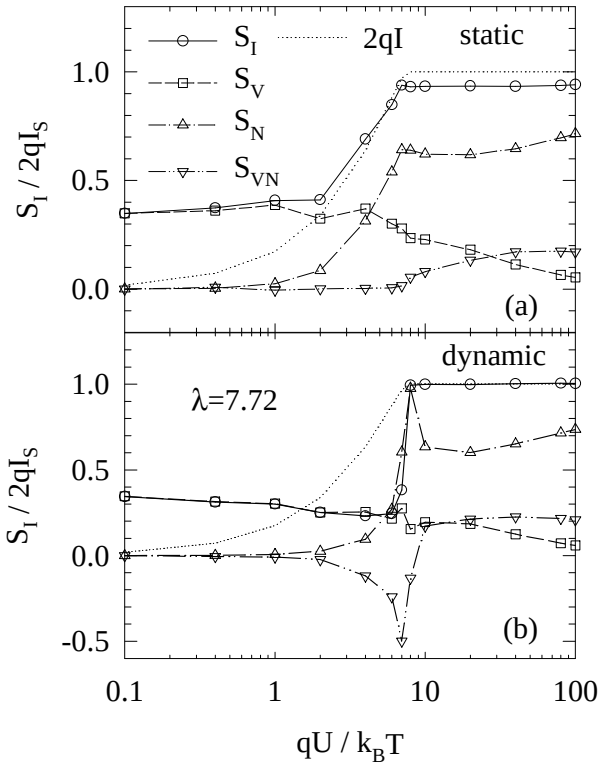

Figure 9. Decomposition of the spectral density of current fluctuations S_I into velocity, number and velocity–number contributions versus applied voltage for the case λ = 7.72 calculated using (a) the static and (b) the dynamic PSs.

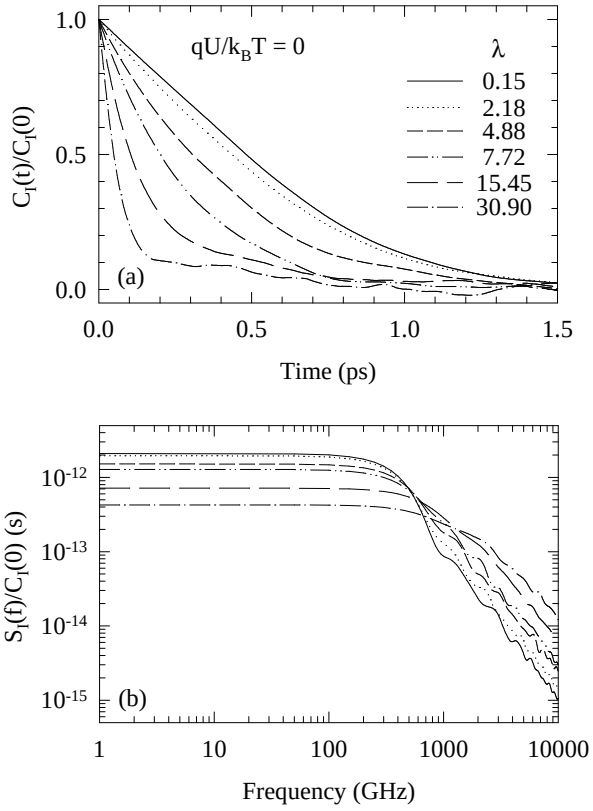

Figure 10. (a) Autocorrelation function and (b) spectral density of current fluctuations at equilibrium for several values of λ. Static and dynamic PSs provide the same results.

the static conductance. In this case, the results for the static (figure 9(a)) and dynamic (figure 9(b)) schemes evidently coincide. However, starting from $qU \sim k_BT$ the difference between the two schemes becomes relevant. For the dynamic case, S_{VN} is negative, while for the static case it is positive. Furthermore, again for the dynamic case, S_N and S_{VN} are of opposite sign and compensate each other, so that S_I^d approximately follows S_V as long as the current is space-charge controlled. As a consequence, the current noise, which now corresponds to shot noise, is considerably suppressed below the value $2qI$ given by the static case. This result reflects the fact that, as the carriers move through the active region, the dynamic fluctuations of the electric field modulate the transmission through the potential minimum and smooth out the current fluctuations imposed by the random injection at the contacts. Therefore, the coupling between number and velocity fluctuations, through S_{VN}, is the main factor responsible for shot-noise suppression. This velocity–number coupling becomes most pronounced just before current saturation ($U \approx 7k_BT/q$), when $V_m \to 0$ and its fluctuations modulate the transmission of the more populated states of the injected carriers (i.e. the low-velocity states). Under current-saturation conditions, space-charge effects no longer modulate the random injection (no potential minimum is present) and again both dynamic and static cases provide the same additive contributions and total noise ($2qI_s$).

3.3. Frequency dependence of noise

In this section we investigate the time and frequency dependence of current fluctuations in the presence of space-charge effects. Figure 10 reports the autocorrelation functions of current fluctuations $C_I(t)$ and the corresponding spectral density $S_I(f)$ under thermal equilibrium conditions at increasing values of λ, thus evidencing the influence of space-charge effects. These results are independent of the PS scheme used. For low values of λ, when V_m is negligible, $C_I(t)$ recovers the typical dependence obtained analytically for the ballistic case when Coulomb interaction is neglected [46, 47]. At increasing values of λ, the shape of $C_I(t)$ changes and tends to exhibit a behaviour determined by two processes with different (short and long) characteristic times. The short time is related to the injected carriers which are not able to pass the potential barrier and return back to the contacts (*returning carriers*). Here, the greater the value of λ, the higher the amplitude of V_m, and the shorter the characteristic *returning time*, as is shown in figure 10(a). The long characteristic time in $C_I(t)$ is associated with the *passing carriers*, whose longitudinal velocity component is significantly reduced while crossing the barrier region. The difference between these two times (and the fraction of reflected/transmitted carriers) becomes more pronounced at high values of V_m. Accordingly, the slopes of $C_I(t)$ related to each time are more easily identified at increasing values of λ. The corresponding spectral densi-

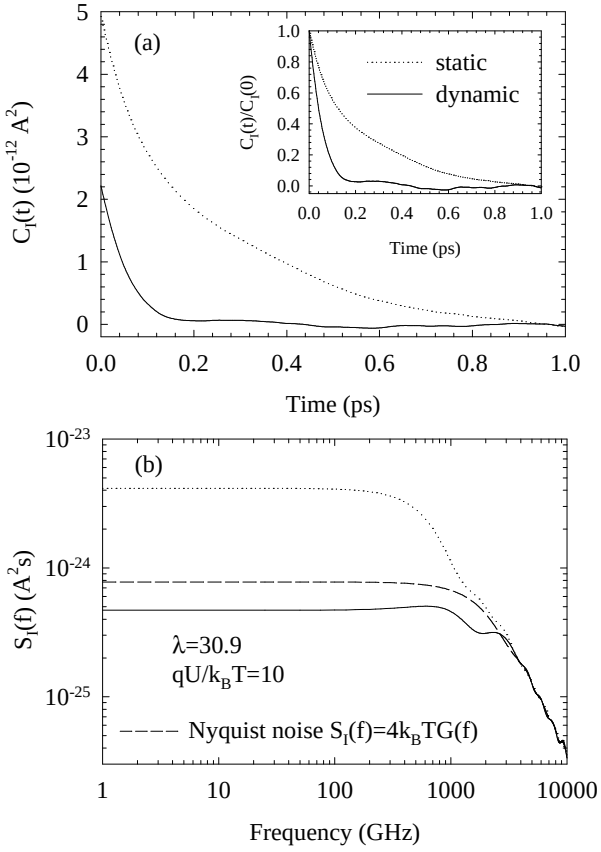

Figure 11. (a) Autocorrelation function (normalized to the zero-time value in the inset) and (b) spectral density of current fluctuations calculated using static and dynamic PSs for the case of $\lambda = 30.9$ and $U = 10k_BT/q$. The cross-sectional area of the structure in the simulation is 2.5×10^{-10} cm^2. Nyquist noise $4k_BTG(f)$ is also shown for comparison in (b).

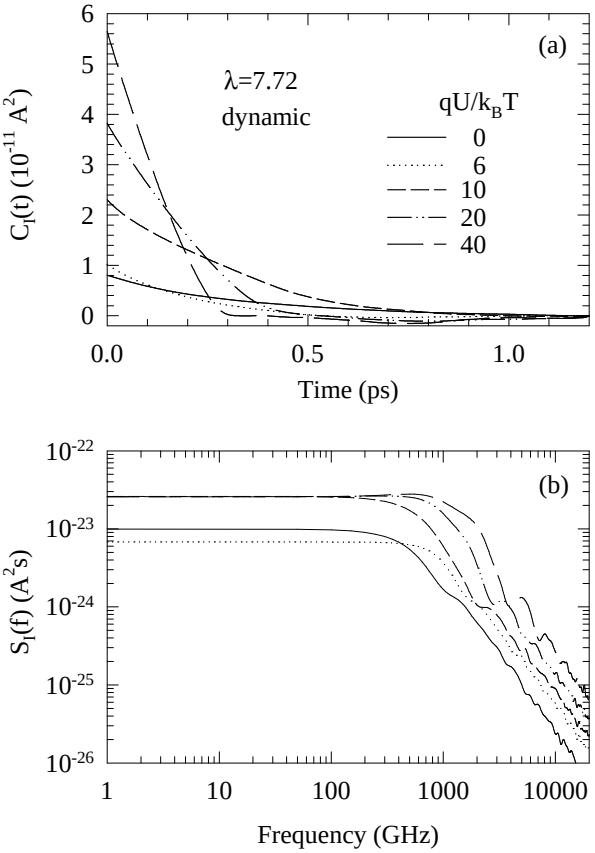

Figure 12. (a) Autocorrelation function and (b) spectral density of current fluctuations calculated using the dynamic PS for the case of $\lambda = 7.72$ at several applied voltages. The cross-sectional area of the structure in the simulation is 4×10^{-9} cm^2.

ties (figure 10(b)) reflect the behaviour of $C_I(t)$ previously described by exhibiting higher cut-off frequencies as λ increases and characteristic structures in the cut-off region related to the transit time through the sample.

To illustrate how the dynamic fluctuations of the self-consistent potential modify the noise in the presence of an applied voltage, figure 11 reports $C_I(t)$ and $S_I(f)$ calculated with the static and dynamic PS for the case of $\lambda = 30.0$ and $U = 10k_BT/q$. Here it can be observed that long-range Coulomb interaction not only reduces the low-frequency amplitude of the noise, but also leads to a different distribution in frequency. The dynamic PS drastically reduces the long time tail of $C_I(t)$ present in the static case (see inset of figure 11(a)). When a static profile of the potential is used, all the carriers with enough energy (higher than qV_m) in the direction of the barrier are able to cross the sample, most of them very slowly (those with an energy close to qV_m). In contrast, in the dynamic case the value of V_m increases with the passage of a carrier, thus blocking the further passage of slower (lower energy) carriers. Moreover, a carrier able to pass the barrier is accelerated by the dynamic redistribution of the potential when crossing the barrier region. Thus, it is mainly fast carriers that contribute to the d.c. current, and the long time tail vanishes. As a consequence, the corresponding spectral density (figure 11(b)), apart from the suppressed value of the plateau, exhibits a higher cut-off frequency in the dynamic case. The expected Nyquist noise $4k_BTG(f)$, with $G(f)$ the differential conductance of the structure calculated at the given applied voltage, is also shown in figure 11(b) for comparison. The Nyquist formula provides an estimation of the noise spectrum which constitutes an intermediate situation between the static and dynamic spectra. The discrepancies between $4k_BTG(f)$ and $S_I(f)$ calculated in the dynamic case clearly indicate the presence of far-from-equilibrium conditions in the structure. Moreover, this comparison demonstrates that the noise obtained using the self-consistent potential is well below (at low frequencies) the Nyquist value, while neglecting Coulomb correlations would lead to an erroneously high value of the noise in the structure under an applied voltage bias. It is remarkable the fact that all three curves exhibit the same values for the highest frequencies after the cut-off, thus demonstrating that the noise in this frequency range is not affected by Coulomb correlations.

Finally, figure 12 shows $C_I(t)$ and $S_I(f)$ calculated with the dynamic PS for the case of $\lambda = 7.72$ at several voltages. Starting from the standard shape of equilibrium

conditions, $C_I(t)$ tends to exhibit a triangular shape, more pronounced as the applied voltage increases. This triangular shape is typical of a constant-velocity emitter with all the electrons reaching the opposite contact [48]. In our case, electrons are injected at the cathode with a velocity which is Maxwellian distributed, but, due to the acceleration provided by the high electric field in the active region, the transit time of all the carriers tends to become practically the same, decreasing with the increase of the applied voltage. The carriers injected at the anode immediately come back to the contact and thus play only an insignificant role at the shortest times. In the spectral density it can be observed that once saturation is reached ($qU > 8k_BT$, see figure 4(a)) $S_I(0)$ takes the same value $2qI_S$ for the different applied voltages, but the spectra after the cut-off are distinguished by showing smoothed *geometrical resonances* at different characteristic frequencies related to the corresponding transit times.

4. Conclusions

We have provided a microscopic analysis of the influence of long-range Coulomb interaction on shot-noise suppression in nondegenerate ballistic transport. To this purpose the carrier dynamics in the active region of a semiconductor structure have been simulated by using an ensemble Monte Carlo technique self-consistently coupled with a PS. A contact model for injecting carriers into the active region which makes use of Poissonian statistics constitutes the origin of shot noise in the current. Several injection rates leading to different levels of space-charge effects inside the active region have been considered. The current–voltage characteristics and other first-order quantities have been investigated and reported in terms of a dimensionless Debye length. Of particular interest, we have found that the current remains almost linear with the applied voltage before saturating at the maximum value a contact can provide. Concerning second-order quantities, the transition from thermal to shot noise in the structure has been analysed. The influence of Coulomb interaction on the noise has been discussed by using static and dynamic schemes to solve the Poisson equation. Under shot-noise conditions, the dynamic fluctuations of the self-consistent potential modify the carrier statistics imposed at the contacts (becoming sub-Poissonian) and are found to be responsible for a remarkable noise suppression, which becomes stronger as space-charge effects become more important. A shot-noise suppression factor decreasing for more than one order of magnitude is predicted. The main contribution to suppression is found to originate from the velocity–number correlations induced by the self-consistent field. The time and frequency dependences of the fluctuations have also been analysed. The noise spectra show different features related to transit time, returning carriers and geometrical resonances, and are also modified by Coulomb correlations among carriers.

The two essential conditions necessary for a relevant shot-noise suppression because of long-range Coulomb interaction are found to be: (i) the presence of a potential barrier which controls the current inside the device and (ii) the dependence on current of the carrier transmission through the barrier. These conditions are quite general and, therefore, the results obtained in the present paper for the case of a space-charge-induced barrier should be extended to a much wider class of physical situations. For example, they could explain some existing controversy between theoretical predictions and experimental measurements in point contacts [26].

Though in principle the shot-noise suppression factor in ballistic transport can be as low as desired by increasing λ, in so doing other kinds of mechanisms, apart from the Coulomb interaction, are expected to become important, e.g. Pauli correlations or scattering processes. In particular, the presence of strong scattering is found to modify the influence of the fluctuating potential on shot-noise suppression [35] and, in some cases, it may become another source of shot-noise suppression [10, 11]. This will be the subject of future investigations.

Acknowledgments

We gratefully acknowledge the support from the NATO networking linkage Grant No. HTECH.LG 960931, the Comisión Interministerial de Ciencia y Tecnología through the project TIC95-0652, the Consejería de Educación y Cultura de la Junta de Castilla y León through the project SA 11/96, and the MADESS II project of the Italian Consiglio Nazionale delle Ricerche (CNR). OMB acknowledges support by the Dirección General de Enseñanza Superior, Spain.

Appendix

The effect of long-range Coulomb interaction in the analysed structures takes place by means of the self-consistent potential $\phi(x)$ calculated at each time step by solving the Poisson equation. Taking into account that the electron concentration in the active region is much higher than the doping ($n(x) \gg n_{ar}$), the Poisson equation takes the form

$$\frac{\mathrm{d}^2\phi(x)}{\mathrm{d}x^2} = \frac{q}{\epsilon}n(x). \tag{A1}$$

By normalizing each of the variables involved in this equation to the corresponding characteristic parameter of the structure: $\tilde{n} = n/n_c$, $\tilde{x} = x/L$ and $\tilde{\phi} = q\phi/k_BT$, the Poisson equation becomes

$$\frac{\mathrm{d}^2\tilde{\phi}(x)}{\mathrm{d}\tilde{x}^2} = \lambda^2\tilde{n}(x) \tag{A2}$$

with λ given by (2). Equation (A2) indicates that the effects related to long-range Coulomb interaction must be identical in structures characterized by the same value of λ. This fact has been corroborated by Monte Carlo simulations.

References

[1] van der Ziel A 1986 *Noise in Solid State Devices and Circuits* (New York: Wiley)
[2] Levitov L S and Lesovik G B 1993 *JETP Lett.* **58** 230
[3] Levitov L S, Lee H and Lesovik G B 1996 *J. Math. Phys.* **37** 4845
[4] Bulashenko O M, Mateos J, Pardo D, González T, Reggiani L and Rubí J M 1998 *Phys. Rev.* B **57** 1366
[5] de Jong M J M 1996 *Phys. Rev.* B **54** 8144
[6] de Jong M J M and Beenakker C W J 1997 *Mesoscopic Electron Transport (NATO ASI Series E: Applied Sciences 345)*, ed L L Sohn, L P Kouwenhoven and G Schön (Dordrecht: Kluwer) p 225
[7] Lesovik G B 1989 *JETP Lett.* **49** 594
[8] Landauer R and Martin T 1991 *Physica* B **175** 167
[9] Shimizu A and Ueda M 1992 *Phys. Rev. Lett.* **69** 1403
[10] Nagaev K E 1992 *Phys. Lett.* A **169** 103
[11] Beenakker C W J and Büttiker M 1992 *Phys. Rev.* B **46** 1889
[12] Landauer R 1993 *Phys. Rev.* B **47** 16 427
[13] Nazarov Y V 1994 *Phys. Rev. Lett.* **73** 134
[14] Büttiker M 1995 *14th Int. Conf. on Noise in Physical Systems and 1/f Fluctuations* ed V Bareikis and R Katilius (Singapore: World Scientific) p 35
[15] de Jong M J M and Beenakker C W J 1995 *Phys. Rev.* B **51** 16 867
[16] Nagaev K E 1995 *Phys. Rev.* B **52** 4740
[17] Kozub V I and Rudin A M 1995 *Phys. Rev.* B **52** 7853
[18] Landauer R 1996 *Physica* B **227** 156
[19] Iannaccone G, Macucci M and Pellegrini B 1997 *Phys. Rev.* B **55** 4539
[20] Blanter Y M and Büttiker M 1997 *Phys. Rev.* B **56** 2127
[21] Li Y P, Zaslavsky A, Tsui D C, Santos M and Shayegan M 1990 *Phys. Rev.* B **41** 8388
[22] Li Y P, Tsui D C, Heremans J J, Simmons J A and Weimann G W 1990 *Appl. Phys. Lett.* **57** 774
[23] Liefrink F, Dijkhuis J I, de Jong M J M, Molenkamp L W and van Houten H 1994 *Phys. Rev.* B **49** 14 066
[24] Liu H C, Li J, Aers G C, Leavens C R, Buchanan M and Wasilewski Z R 1995 *Phys. Rev.* B **51** 5116
[25] Birk H, de Jong M J M and Schönenberger C 1995 *Phys. Rev. Lett.* **75** 1610
[26] Reznikov M, Heiblum M, Shtrikman H and Mahalu D 1995 *Phys. Rev. Lett.* **75** 3340
[27] Kumar A, Saminadayar L, Glattli D C, Jin Y and Etienne B 1996 *Phys. Rev. Lett.* **76** 2778
[28] Steinbach A H, Martinis J M and Devoret M H 1996 *Phys. Rev. Lett.* **76** 3806
[29] Schoelkopf R J, Burke P J, Kozhevnikov A A, Prober D E and Rooks M J 1997 *Phys. Rev. Lett.* **78** 3370
[30] Yau S T, Sun H B, Edwards P J and Lynam P 1997 *Phys. Rev.* B **55** 12 880
[31] Schoelkopf R J, Kozhevnikov A A, Prober D E and Rooks M J 1998 *Phys. Rev. Lett.* **80** 2437
[32] Reklaitis A and Reggiani L 1997 *J. Appl. Phys.* **82** 3161
[33] González T, González D, Mateos J, Pardo D, Reggiani L, Bulashenko O M and Rubí J M 1998 *Phys. Rev. Lett.* **80** 2901
[34] González T, Bulashenko O M, Mateos J, Pardo D and Reggiani L 1997 *Phys. Rev.* B **56** 6424
[35] González T, Bulashenko O M, Mateos J, Pardo D, Reggiani L and Rubí J M 1997 *Semicond. Sci. Technol.* **12** 1053
[36] van der Ziel A and Bosman G 1982 *Phys. Status Solidi* A **73** K93
[37] Naveh Y, Averin D V and Likharev K K 1997 *Phys. Rev. Lett.* **79** 3482
[38] Nagaev K E 1998 *Phys. Rev.* B **57** 4628
[39] Thompson B J, North D O and Harris W A 1940 *RCA Rev.* **4** 269
Thompson B J, North D O and Harris W A 1940 *RCA Rev.* **4** 441
[40] van der Ziel A 1954 *Noise* (Englewood Cliffs, NJ: Prentice-Hall)
[41] González T and Pardo D 1993 *J. Appl. Phys.* **73** 7453
[42] Reggiani L, Kuhn T and Varani L 1992 *Appl. Phys.* A **54** 411
[43] Reggiani L, Golinelli P, Faucher E, Varani L, González T and Pardo D 1995 *Noise in Physical Systems and 1/f Fluctuations* ed V Bareikis and R Katilius (Singapore: World Scientific) p 163
[44] Reggiani L, Varani L, González T, Pardo D and Kuhn T 1995 *Proc. 22nd Int. Conf. on the Physics of Semiconductors* ed D J Lockwood (Singapore: World Scientific) p 1963
[45] Greiner A, Kuhn T, Reggiani L and Varani L 1997 (unpublished)
[46] Stanton C J and Wilkins J W 1985 *Physica* B **134** 255
[47] Varani L, Reggiani L, Houlet P, Vaissere J C, Nougier J P, Kuhn T, González T and Pardo D 1994 *Semicond. Sci. Technol.* **9** 584
[48] Kuhn T, Reggiani L and Varani L 1992 *Superlatt. Microstruct.* **11** 205